Ab Initio Studies on the Mechanism of Tyrosine Coupling

Igor L. Shamovsky,*,† Richard J. Riopelle,† and Gregory M. Ross‡

Department of Medicine, and Department of Physiology, Queen's University, Kingston, Ontario, Canada K7L 2V7

Received: October 9, 2000; In Final Form: December 11, 2000

Oxidative stress is considered to be a major contributor to dysfunction in a host of disease states. Reactive oxygen species (ROS) mediate distinct oxidative alterations in biopolymers, including DNA, proteins, lipids, and lipoproteins. Currently, the mechanisms of biochemical reactions underlying oxidative stress are poorly understood because of the instability of ROS. One of the consequences of oxidative stress is one-electron oxidation of tyrosine (Tyr) residues in proteins, which represents a hallmark of this insult and is implicated in the pathogenesis of a number of pathological processes leading to atherosclerosis, inflammatory conditions, multiple system atrophy and several neurodegenerative diseases. Major products of oxidation of Tyr include protein-bound dityrosine and isodityrosine. In this report, the mechanism of tyrosine coupling (including structure and stability of a number of proposed reaction intermediates) is studied by high-level density functional and conventional ab initio methods including B3LYP, MP2, CASSCF, and CASPT2. It is demonstrated that dityrosine and isodityrosine are the most stable structures at all theoretical levels applied. In addition to classical structures of the reaction intermediates, evidence is found for a novel transient structure of Tyr dimer, stacked dityrosyl. This dimer is predicted to exist because of strong electron correlation between two tyrosyl moieties. The counterpoise corrected energy of stacked dityrosyl is below the energy of two tyrosyl radicals by about 95 kJ/mol at the PUMP2/6-31G** level. High proton affinity of tyrosyl radical (about 9.4 eV) suggests that positively charged amino acids in the vicinity of a solvent-exposed Tyr residue may increase the probability of tyrosine coupling.

Introduction

Recent experimental data suggest that oxidative stress triggers several biochemical mechanisms leading to aging, as well as a variety of pathological processes.[1−6] Examples of pathological conditions where oxidative stress may play a role include cancer,[7] atherosclerosis,[8] inflammatory conditions,[9] stroke,[10] amyotrophic lateral sclerosis,[11] and multiple sclerosis.[12] It has also been implicated in a host of neurodegenerative diseases, including Alzheimer's, Parkinson's, and Huntington's diseases.[5,6,9−18] Oxidative processes result in characteristic chemical modifications in DNA, proteins, lipids, and lipoproteins. Oxidative stress is frequently mediated by reactive oxygen species (ROS), which may include superoxide anion ($^{\bullet}O_2^-$), singlet oxygen ($^1O_2$), hydroxyl radical ($^{\bullet}OH$), alkoxy radical ($^{\bullet}O-R$), hydroperoxyl radical ($^{\bullet}OOH$), peroxyl radical ($^{\bullet}OO-R$), tyrosyl radical (Tyr-O$^{\bullet}$), carbonate radical anion ($^{\bullet}CO_3^-$), nitrogen dioxide radical ($^{\bullet}NO_2$), hypochlorite anion (OCl^-), peroxynitrite anion ($ONOO^-$), and peroxynitrous acid (ONOOH).[10,15−24] In neurodegenerative diseases and stroke, oxidative stress is a major part of the more complicated interrelated set of mechanisms leading to neuronal cell death, which constitutes the lethal triplet of oxidative stress, metabolic compromise, and glutamate excitotoxicity.[25]

A typical feature of oxidative stress in the physiological pH range is the formation of tyrosyl radicals (**II**) by abstraction of hydrogen atom from the hydroxyl group of tyrosine (Tyr, **I**) by ROS (Figure 1).[26−28] Protein-bound dityrosine, a major product of Tyr modification in proteins, is formed by recombination of two tyrosyl radicals (Figure 2).[15,24,28−36] Tyrosine coupling is an irreversible process which may lead to intermolecular cross-links and/or wide intramolecular loops in proteins and lipoproteins, thereby initiating their dysfunction and aggregation.[24,28,30,36,37] Tyrosine coupling is believed to be a prime marker of oxidative stress in atherosclerosis, inflammatory conditions, and neurodegenerative diseases.[24,30,33,36,38] Two structures of dityrosine have been identified (Figure 2), 3,3′-dityrosine (dityrosine, **III**) and 3-[4′-(2-carboxy-2-aminoethyl)phenoxy]tyrosine (isodityrosine, **IV**).[24] Tyrosine coupling is one example of a more general process of oxidative coupling of phenols, which is abundant in nature.[37,39]

Mechanisms of biochemical reactions underlying oxidative stress are poorly understood because of the instability of the radical species involved. The structure of reaction intermediates and mechanisms of chemical transformations remain hypothetical, and are often devised from the structure of the identified products of oxidation of biopolymers.[24,39,40] This approach alone is not able to lead to the exact reaction mechanisms, nor to explain the remarkable regio- and stereoselectivity of radical oxidative reactions which is frequently observed.[22,26,39,41,42] For this reason, ab initio theory represents a useful tool in studying the mechanisms of biochemical reactions mediated by ROS.

In this report, we study the mechanism of tyrosine coupling by ab initio and density functional methods in the gas phase. This study includes putative processes of formation of tyrosyl radical (Figure 1) and their subsequent recombination (Figure 2). In addition to classical reaction intermediates (**V** and **VI**),[24]

* Author to whom correspondence should be addressed: Dr. Igor L. Shamovsky, Department of Medicine, Apps Medical Research Center, #6-305, DORAN-3, KGH, Kingston, Ontario, Canada K7L 2V7. Tel: (613) 549-6666, ext. 4433. Fax: (613) 548-1369. E-mail: is3@post.queensu.ca.

† Department of Medicine, Queen's University.

‡ Department of Physiology, Queen's University.

10.1021/jp003693e CCC: $20.00
Published on Web 01/20/2001

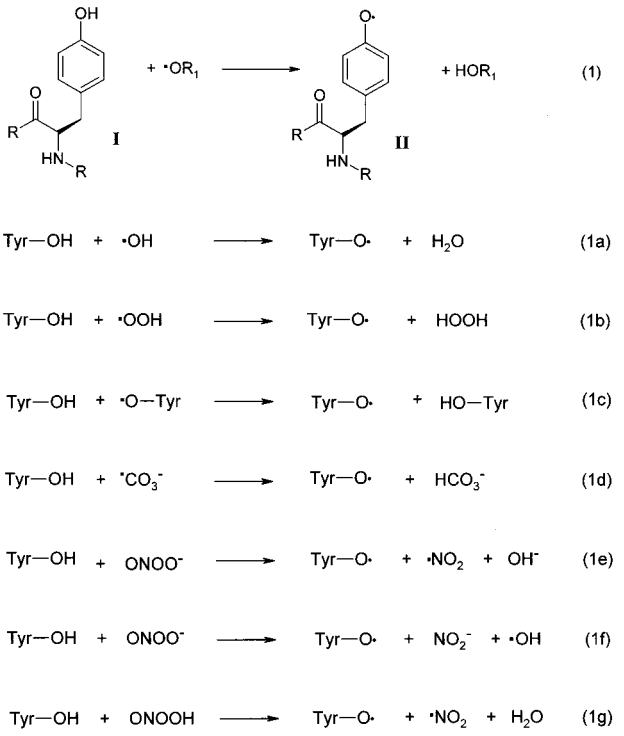

Figure 1. Putative reactions of formation of neutral tyrosyl radical (**II**) from neutral Tyr (**I**) in the physiological pH range.

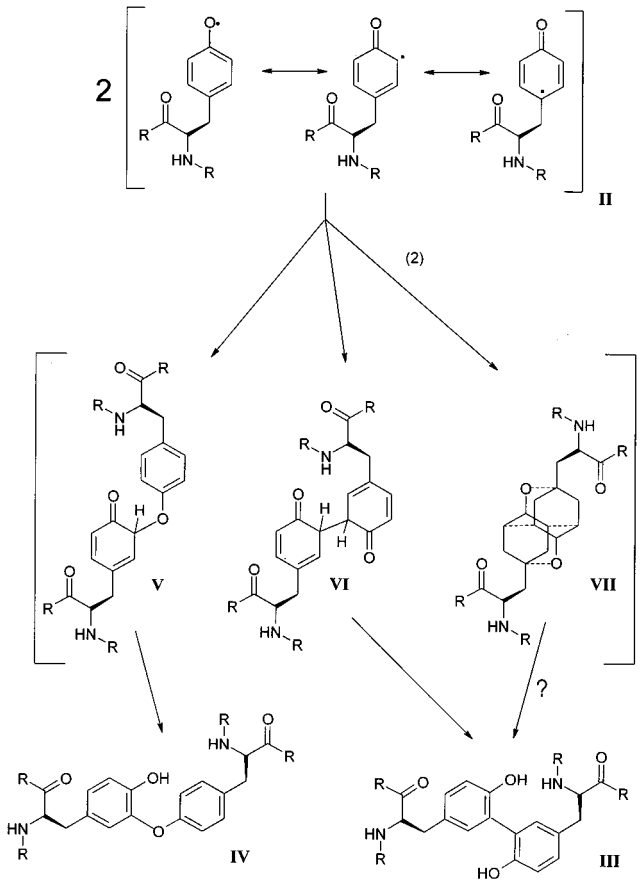

Figure 2. Putative reaction pathways for tyrosine coupling. Structure **II** − tyrosyl radical; structures **III** (dityrosine) and **IV** (isodityrosine) − products of tyrosine coupling; structures **V**−**VII** − reaction intermediates. Question mark designates a tentative reaction pathway of the predicted transient intermediate **VII**.

a novel transient structure of dityrosine, stacked dityrosyl (**VII**), is predicted (Figure 2). Electron correlation is demonstrated to play the central role in stabilizing stacked dityrosyl, particularly because the HOMO electron pair in this dimer is highly delocalized (over 10 atoms). Phenoxyl radical is regarded as a notoriously difficult open-shell system requiring multi-determinant consideration.[43,44] It has been further demonstrated that the correct description of the excited states of tyrosine also requires multi-determinant wave functions.[45] We demonstrate here that the ground state of phenoxyl and tyrosyl radicals can be described adequately at the PUMP2 level, as the multi-determinant description of the wave function is not required for geometry and energetics. The dynamic electron correlation effects are dominant in stacked diphenoxyl and dityrosyl, therefore, these molecules represent a challenge for modern computational chemistry and computational power.

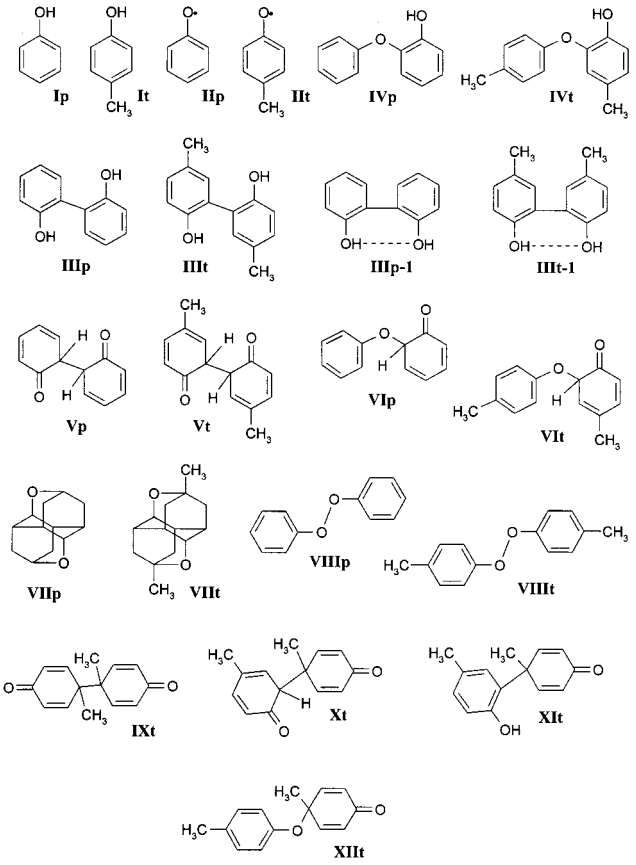

Figure 3. Structures of the molecules under study. Index **p** designates derivative of phenol, index **t** designates *p*-cresol.

Methods

Since chemical transformations associated with tyrosine coupling are localized within phenolic rings of Tyr residues (reactions 1 and 2), these reactions were studied using smaller systems derived from phenol and *p*-cresol, without peptide backbones (Figure 3). Structure and stability of the initial species (**I** and **II**), the observed products (**III** and **IV**), and a variety of hypothetical reaction intermediates (**V**−**XII**) of tyrosine coupling (Figure 3) were studied by fully optimized density functional theory (DFT)[46,47] and conventional ab initio calculations using the split-valence 6-31G** basis set.[48] The DFT calculations utilized the Becke's three-parameter exchange functional with the Lee−Yang−Parr's correlation functional (B3LYP).[49,50] This particular hybrid GGA functional is the most widely used, and has been demonstrated to yield remarkable accuracy in structure, dipole moments, thermochemistry, and vibrational frequencies in various molecular systems.[51] Con-

TABLE 1: Comparison of Theoretically and Experimentally Obtained OH Bond Strengths (in kJ/mol) in Reference Molecules

	level of theory[a]				
molecule	B3LYP/6-31G**	PUMP2/6-31G**	CASSCF/6-31G*	CASPT2/6-31G*	experiment[61]
H−OH	501.4	493.5			498 ± 4
H−OCH_3	444.6	452.2			436.0 ± 3.8
H−O_2H	364.7	375.6			369.0 ± 4.2
H−O_2CH_3	359.2	373.4			370.3 ± 2.1
H−OC_6H_5	375.0	376.2	**253.4**	377.3	361.9 ± 8

[a] Bond strengths of OH groups in indicated molecules were determined using ab initio calculations at different levels of theory by estimating the energy required for its homolytical dissociation. Full geometry optimizations were performed at the B3LYP, UMP2, and CASSCF levels, the CASPT2 (CASSCF-MP2) energy was calculated with the CASSCF-optimized geometry. The full π-electron active space was used in CASSCF and CASPT2 methods, i.e., full configuration interaction of 8 and 7 π-electrons was taken into account in phenol (C_6H_5OH) and phenoxyl radical ($C_6H_5O^{\bullet}$), respectively, in a subset of 7 π-MO. All theoretical levels presented, except for CASSCF/6-31G* (underlined bolded value), demonstrate marked accuracy in OH bond strengths in the molecules under study. Taking the zero-point energy (ZPE) correction of the OH bond strength in phenol into account decreases the predicted values approximately by 33 kJ/mol.

ventional ab initio methods of correlation energy correction, namely frozen-core unrestricted second-order Møller−Plesset perturbation theory (UMP2),[52,53] complete active space multiconfiguration self-consistent field (CASSCF),[54] and CASSCF with a full MP2-level electron correlation correction (CASPT2),[55] were used to support predictions made in the present study based on the DFT calculations. To avoid possible problems with size consistency within the CASSCF(2,2) and CASPT2(2,2) approaches when evaluating dimerization energy of phenoxyl radical, the energy of the monomer was calculated after splitting of the dimer into two noninteracting (separated by 20 Å) monomers.

Restricted open-shell Hartree−Fock (ROHF)[56] and unrestricted Hartree−Fock (UHF)[57] calculations were carried out to demonstrate a pivotal role of electron correlation effects in **I** and **VII**. "Projection" (P) of unrestricted wave functions was utilized to remove contaminants from higher spin states from UHF and UMP2 wave functions of doublet states by means of spin projection operators;[58] the resulting PUHF and PUMP2 energies were used to predict energetics of chemical transformations involving radical species. Geometry optimizations of symmetrical molecular systems at the B3LYP and UMP2 levels were followed by calculations of normal frequencies to identify the nature of the stationary points. To demonstrate stability of novel reaction intermediates, stacked diphenoxyl and stacked dityrosyl, basis set superposition errors (BSSE) were evaluated by computation of the counterpoise corrections.[59] The influence of zero-point vibrational energies on relative stabilities of the molecular systems under study was not investigated because of complexity of the systems and since the obtained ab initio results agree well with available experimental data. Ab initio calculations were performed with the program Gaussian-98[60] on an IBM SP2 high-performance computer available through the High Performance Computing Virtual Laboratory (HPCVL) at Queen's University at Kingston.

Results and Discussion

Formation of Tyrosyl Radical. Tyrosyl radical has been demonstrated to result from the abstraction of hydrogen atom from the OH group of Tyr by ROS at physiological pH.[26−28] This process is caused by the relative stability of the phenoxyl radical nucleus (**IIp**, Figure 3),[39] such that the bond strength of the phenolic hydroxyl appears to be less than or equal to the resulting stabilization of ROS. While methods of computational chemistry are currently unable to demonstrate whether a particular reaction is involved in oxidative stress processes, it is possible to recognize improbable reaction pathways which are accompanied by significant increase in energy.[61] To identify those pathways, it is critical to establish the theoretical level which allows one to reproduce fundamental experimental data, e.g., the bond strength of hydroxyl groups in a set of test molecules, such as H_2O, CH_3OH, HOOH, CH_3OOH, and C_6H_5-OH.

Table 1 presents the OH bond strengths in the test molecules obtained by fully optimized ab initio calculations. These data indicate that both UB3LYP/6-31G** and PUMP2/6-31G** levels are able to reproduce the experimental results with remarkable precision. Mean relative error of the predicted OH bond strengths in the test molecules is 0.4% and 1.9%, respectively, for these methods. The influence of zero-point vibrational energies on the OH bond strength of phenol is relatively insignificant (Table 1). Surprisingly, the more sophisticated method, full π-electron space CASSCF,[44] fails to reproduce the OH bond strength in phenol, as it underestimates the stabilization energy of phenol with respect to that of phenoxyl radical. The disagreement of the full π CASSCF/6-31G* prediction with experimental and other theoretical results is eliminated by taking into account $\sigma-\pi$ dynamic correlation using MP2 perturbation theory correction within each electron configuration of the active space in the framework of the CASPT2 approach (Table 1). Particularly, "projected" wave function PUMP2 describes the energy difference between phenol and phenoxyl radical as good as the multi-determinant CASPT2 functional. A similar effect has previously been detected when studying the single−triplet split in cyclobutadiene.[43] This result indicates that electron correlation effects in phenol are significantly underestimated by the π CASSCF approach because the wave function does not include correlation between σ and π electrons. Moreover, if correlation between π electrons is also neglected (within the PUHF approach), phenol is further destabilized and, accordingly, the predicted OH bond strength decreases to 114.6 kJ/mol versus an experimental value of 361.9 ± 8 kJ/mol.[62] It has been previously found that the optimized geometric features of phenoxyl radical are very similar when using UMP2 and full π CASSCF methods.[51a] These striking results suggest that dynamic electron correlation in phenolic systems is very strong, and this is the correlation within both σ- and π-electron systems (but not variational multireference description of wave function by itself), which is absolutely critical for geometry and stability. Since the HOMO π-electron pair is separated when abstracting H from phenol, correlation between these particular electrons in phenol are most important for a correct description of the dissociation energy.[61] The reason for the significance of correlation of this particular electron pair in phenol (Table 1) is high delocalization of the corresponding MO (HOMO).[43] Both single-determinant UB3LYP/6-31G** and PUMP2/6-31G** levels of theory appear to be sufficient to take this effect into account (Table 1).

TABLE 2: Energy of Selected Reactions of One-Electron Oxidation of *p*-Cresol (molecule It) by Reactive Oxygen Species As Predicted by Fully Optimized DFT and ab Initio Calculations[a]

	level of theory	
reaction[b]	B3LYP/6-31G**	PUMP2/6-31G**
1a	−134.0	−119.9
1b	2.7	−2.0
1c	0.0	0.0
1d	−12.4	2.1
1e	240.9	204.4
1f	108.7	96.7
1g	−38.8	−57.3

[a] In kJ/mol. Each molecule was represented by its minimum-energy conformation. [b] Reaction equations are presented in Figure 1 where tyrosine (**I**) is simulated by a smaller molecule **It** (Figure 3).

The *p*-alkyl substituent in cresol (similar to Tyr) slightly weakens the OH bond, which is consistent with the observation that *p*-cresol demonstrates lower redox potential than phenol at neutral pH.[63] According to the B3LYP/6-31G** and PMP2/6-31G** calculations, the OH bond strength is lower in **It** than in **Ip** by 7.6 and 2.6 kJ/mol, respectively. This means that the *p*-alkyl group somewhat stabilizes the phenoxyl radical in Tyr. Table 2 provides the potential energy balance of the proposed reactions of one-electron oxidation of Tyr (simulated with molecule **It**) by ROS (Figure 1). The results indicate that reactions 1e and 1f are improbable at room temperature, because the predicted stabilization of peroxynitrite ($ONOO^-$) as a result of a one-electron reduction is much lower than the energy required to abstract H from the OH bond in **It**. The estimated peroxynitrite stabilization according to pathway (1f) is around −280 kJ/mol, which is significantly lower by absolute value than the OH, CH, and SH bond strengths (>310 kJ/mol) in natural molecular species (e.g., phenolic compounds, unsaturated fatty acids and cysteine residues) which are generally affected in oxidative radical reactions.[10] This result suggests that peroxinitrite anion is not likely a direct mediator of natural oxidative radical reactions.[19] Alternatively, the protonated form of peroxynitrite, peroxynitrous acid (ONOOH), is a much more potent oxidizer than peroxynitrite. The predicted energy of stabilization of ONOOH during one-electron reduction according to the currently accepted pathway (1g)[19] is estimated to be −406.3, −437.3, −446.2, and −455.5 kJ/mol at the B3LYP/6-31G**, B3LYP/6-311+G(2d,p), PMP2/6-31G**, and PMP2/6-311+G(2d,p) levels, respectively, which is much higher than the energy required for breaking the OH bond in phenolic compounds (approximately 360 kJ/mol;[62] Table 1). These considerations suggest that the active form of peroxynitrite in oxidative radical processes at physiological pH is peroxynitrous acid, which is consistent with recent experimental studies on the pH dependence of the oxidative activity of peroxynitrite on dopamine,[17] melatonin,[64] and tyrosine.[65]

The predicted energy of reactions of one-electron oxidation of Tyr by other forms of ROS (Figure 1, Table 1) is consistent with their direct involvement in the formation of tyrosyl radicals. Specifically, the present results support the recently suggested concept that both carbonate radical anion ($^{\bullet}CO_3^-$)[22,34,66,67] and tyrosyl radical (Tyr-O$^{\bullet}$)[15,24,30] are important ROS, and explain their more selective reactivity with respect to hydroxyl radical and peroxynitrous acid.[15,22,24,34]

Since the height of the energy barrier hindering hydrogen atom transfer from Tyr to ROS determines the rate of this chemical transformation, the existence of the energy barriers within the intrinsic reaction pathways (IRP) with the selected ROS (Figure 1) was investigated by DFT and ab initio calculations. Geometric features of the complex of **It** with different ROS were fully optimized starting with geometries of the optimized separate molecules in order to find the energy minimum corresponding to the H-bonded complex Tyr-OH··· ROS preceding hydrogen transfer. The existence of such energy minimum within the IRP would indicate the presence of a barrier hindering the hydrogen transfer, because in this case the abstraction of H from Tyr-OH would be accompanied with the energy increase. It is found that such an H-bonded complex does not exist within the IRP of Tyr with $^{\bullet}OH$ as the energy of the H-bonded complex gradually decreases when H is separated from Tyr-OH and bind to $^{\bullet}OH$ at both B3LYP/6-31G** and MP2/6-31G** levels of theory, which suggests that there is no barrier for hydrogen transfer in the reaction pathway 1a. On the other hand, the H-bonded complexes prior to hydrogen transfer are identified within IRP of **It** for less exothermic reactions with $^{\bullet}OOH$, Tyr-O$^{\bullet}$, and ONOOH at both the B3LYP/6-31G** and MP2/6-31G** levels. This result is consistent with Semyonov-Polanyi's law,[68] which states that the barrier of the reaction increases when heat decreases. The B3LYP/6-31G** fully optimized structures of the hydrogen-bonded complexes preceding hydrogen transfer in reactions 1b, 1c, and 1g are illustrated in Figure 4. Neither identified equilibrium hydrogen-bonded structure possesses any element of symmetry.

Tyrosine Coupling. Table 3 presents relative energies of different structures along the pathway of recombination of two tyrosyl radicals (Figure 3). All of these dimers correspond to local energy minima at the B3LYP/6-31G** and MP2/6-31G** levels. As one would expect, the observed products of Tyr coupling, dityrosine (**III**) and isodityrosine (**IV**), are considerably more stable than the other dimeric structures. According to the B3LYP results (Table 3), all structures derived from tyrosyl radicals, except for **VIIt** (i.e., **IIIt**−**VIt** and **VIIIt**), are significantly less stable than corresponding structures derived from phenoxyl radicals. The nature of this destabilization is likely to be closely related to the weakening of the OH bond by the *p*-alkyl substituent (as demonstrated above). This being the case, the B3LYP/6-31G** energy of dimers of tyrosyl radicals has to be higher than those of phenoxyl radicals by approximately 15.2 kJ/mol. As is seen in Table 3, this is the case for the dimers possessing two benzene rings, namely, for both major products of Tyr coupling, **III** and **IV**, and the hypothetical structure **VIII**. Deviation from this trend increases in reaction intermediates as the number of the benzene rings with broken aromaticity increases: **VI** (one ring) < **V** (both rings). The higher stability of **VIIt** with respect to **VIIp** predicted by the B3LYP and MP2 methods is a result of the weak H-bonding CH···O═C between the methyl group and the phenolic oxygen belonging to the different phenoxyl units in **VIIt**.

All dimeric structures analyzed appear to be more stable at the MP2 than at the B3LYP level (Table 3), probably because the MP2 method is usually characterized by higher magnitudes of BSSE. The average difference in predicted stabilities of the dimers of phenoxyl radicals at the PUMP2/6-31G** and UB3LYP/6-31G** levels is −67.6 ± 6.1 kJ/mol. The dimer in which phenoxyl radicals are in stacked arrangement (stacked dityrosyl, **VII**) demonstrates the maximal difference, −113.3 and −127.7 kJ/mol for **VIIp** and **VIIt**, respectively. The considerable difference in predictions of the MP2 and B3LYP methods with respect to the stability of **VII** is due to the recognized general inability of DFT methods to describe intermolecular attractive dispersion interactions,[51g,69] which are dominant in stacking complexes of planar molecules.[51j] Specif-

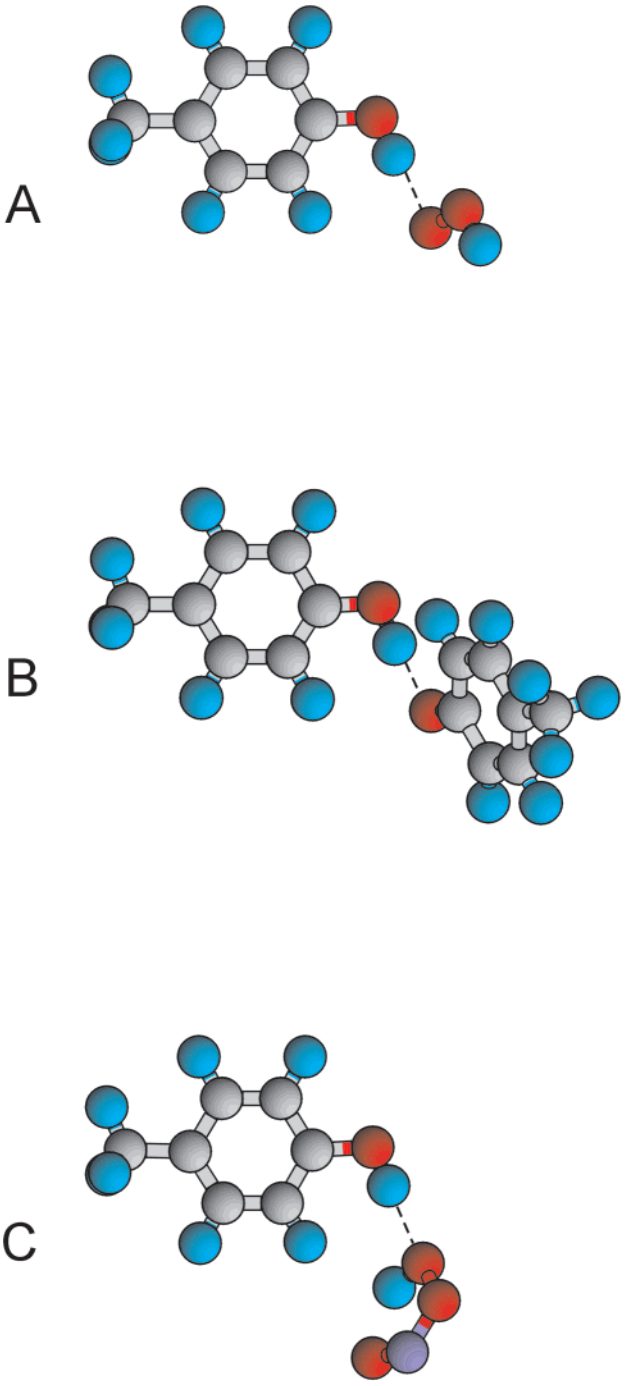

Figure 4. Structures of hydrogen-bonded complexes of *p*-cresol with ROS obtained by fully relaxed DFT calculations at the B3LYP/6-31G** level. A − with hydroperoxyl radical; B − with tyrosyl radical; C − with peroxynitrous acid. Broken lines designate hydrogen-bonds. According to the B3LYP/6-31G** level of theory, no barrier hindering the hydrogen atom abstraction from *p*-cresol exists for hydroxyl radical, which is consistent with its extreme oxidative power. Gray, red, purple and blue spheres designate carbon, oxygen, nitrogen, and hydrogen atoms, respectively.

ically, the B3LYP method has been found to significantly underestimate the stabilization energy of the stacked nucleic acids.[70] This makes the MP2 approach the only currently available tool to reasonably predict the structure and stability of **VII**. The other ab initio methods which more rigorously treat dynamic correlation effects will require enormous computational resources. The BSSE correction results in the decrease of the predicted stabilities of **VII** presented in Table 3; the counterpoise

TABLE 3: Relative Stabilities (in kJ/mol) of the Different Dimeric Structures Derived from Tyrosyl Radicals As Predicted by Fully Optimized DFT and ab Initio Calculations[a]

	level of theory				
	UB3LYP/6-31G**			PUMP2/6-31G**	
	model[b]			model[b]	
molecule[b]	**p**	**t**	**t−p**	**p**	**t**
III	−224.7	−209.7	15.0	−308.6	
III-1	−243.4	−229.3	14.1	−327.7	
IV	−210.1	−196.2	13.9	−273.0	
V	−53.1	−48.6	4.5	−126.9	
VI	−94.5	−85.5	9.0	−153.0	
VII	−15.9	−20.8	−4.9	−129.2	−148.5
VIII	24.2	37.7	13.5	−18.1	
IX		−12.2			
X		−31.3			
XI		−110.1			
XII		−90.4			

[a] Energy of two isolated tyrosyl radicals (modeled either by **IIp** or **IIt**) was considered as zero. [b] Structures of the molecules are illustrated in Figure 3. Molecules **IXp**−**XIIp** were not considered as the methyl group is critical for energetics and chemical reactivity of **IXt**−**XIIt.** The BSSE correction is not shown.

corrected PUMP2/6-31G** energies of **VIIp** and **VIIt** are of considerable magnitude, −80.2 and −94.6 kJ/mol, respectively, which allows us to suggest molecule **VII** as a putative reaction intermediate of Tyr coupling leading to dityrosine **III** (Figure 2). The predicted stabilities of the reaction intermediates underlying the reaction pathway of Tyr coupling is illustrated in Figure 5. Fully optimized geometries of the products and reaction intermediates of tyrosine coupling are illustrated in Figure 6.

As the structure of stacked dityrosyl (**VII**) has not been previously described, we studied this molecule using a more detailed theoretical analysis. Figure 7 illustrates the bonding diagram of two phenoxyl radicals in a stacked arrangement. The HOMO of **VIIp** (symmetry a_g) is formed from the symmetrically compatible SOMO's of two phenoxyl radicals (each of symmetry b_1). Molecule **VIIp** belongs to the C_{2h} group of symmetry, the electron state of this molecule is ^1A_g. Figure 8 shows the HOMO of **VIIp** as obtained at the HF/6-31G** level using the MP2/6-31G** optimized geometry. As seen, the HOMO electron pair which is responsible for binding of the two phenoxyl units (Figure 7) is delocalized over 10 atoms (eight carbons and two oxygens); this indicates that correlation of these particular electrons has to play a particularly significant role in stabilization of **VII**.

Dimerization energy and optimized geometric features of this molecule predicted at the different levels of theory are presented in Table 4. As one would expect, the predicted stability of **VII** is, in fact, highly dependent on the utilized theoretical level, as they vary in ability to recover electron correlation energy. Remarkably, there is no stabilization in **VII** at the Hartree−Fock levels of theory. Hence, chemical bonding within the stacked dimer of phenoxyl radical is exclusively due to electron correlation effects, similar to F_2. As demonstrated above, the full π CASSCF approach considerably underestimates dynamic correlation effects in phenol, because it neglects $\sigma-\pi$ correlation. This is the case for **VII**, in particular, because of the extraordinary delocalization of the HOMO. Correspondingly, the CASSCF(2,2) and CASSCF(10,10) methods significantly underestimate the dimerization energy of **VII** in comparison with the PUMP2 prediction (Table 4). The latter approach, however, is potentially affected by residual spin contamination

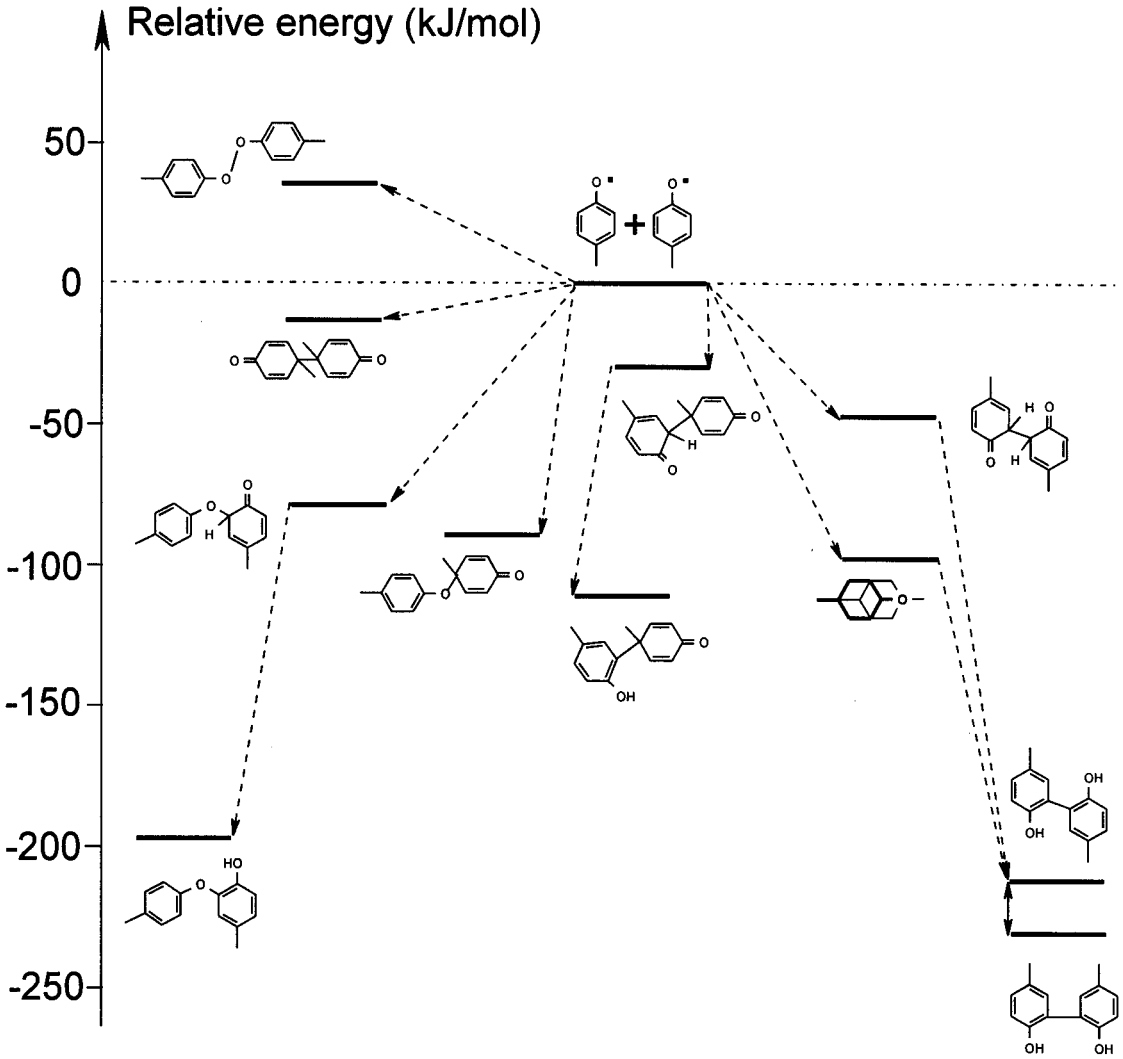

Figure 5. Proposed energy diagram for tyrosine coupling according to DFT calculations at the B3LYP/6-31G** level. Tyrosine was simulated by *p*-cresol. Energy of stacked dityrosyl was obtained by counterpoise-corrected PUMP2/6-31G** calculations.

in phenoxyl radical,[43,44c] which may lead to an artifactual stabilization of the dimer, even though this effect does not appear to be significant when evaluating the OH bond strength in phenol (Table 1). The combination of the two approaches, CASSCF(2,2) and MP2, is one possible way to avoid this problem. The three-determinant CASPT2(2,2) method ensures that the resulting wave functions of both monomer (**IIp**) and dimer (**VIIp**) are eigenvectors of operators $\mathbf{S}^2$, and that dynamic electron correlation effects in **VIIp** are taken into account. The first component (CASSCF) of this combined approach recovers static electron correlation, whereas the second (MP2) evaluates dynamic electron correlation effects including $\sigma-\pi$ correlation. The CASPT2(2,2)/6-31G** energies were calculated on the basis of the geometries of both monomer and dimer which were obtained by full geometry optimization at the CASSCF(2,2)/6-31G** level. The enormous difference between dimerization energies of phenoxyl radical predicted by the CASSCF(2,2) and CASPT2(2,2) methods (Table 4) confirm that dynamic electron correlation effects in **VII** are, in fact, extremely important. Calculations of vibrational frequencies reveal that stacked phenoxyl (**VIIp**) with the C_{2h} symmetry corresponds to the energy minimum only at correlated levels, i.e., MP2/6-31G* and B3LYP/6-31G**, whereas it is the transition state with one imaginary frequency at the HF/6-31G** level.

The geometry of **VII** is also strongly affected by dynamic electron correlation. Figure 9 presents the optimized bond lengths for monomer (**Ip**) and dimer (**VIIp**) of phenoxyl radical obtained by different theoretical approaches using the same basis set (6-31G**). Results indicate that dimerization leads to significant geometric changes in phenoxyl moieties, but in the opposite directions, depending on whether the electron correlation is neglected or included (Figure 9). The UHF method predicts that dimerization changes phenoxyl moieties toward the quinoid ring type, whereas CASSCF(2,2) and UMP2 methods predict a trend toward a benzenoid system. The B3LYP results are intermediate, as they demonstrate no significant bond length changes. The rms-differences between the optimal bond lengths within phenoxyl moieties in **IIp** and **VIIp** (Figure 9) predicted by the set of four fully relaxed ab initio techniques are presented in Figure 10. The underlined rms magnitudes in Figure 10 signify geometric similarity. These data reveal the basis for conflicting geometric predictions made by the different theoretical approaches. In phenoxyl radical, CASSCF(2,2) and UMP2 geometric predictions are very similar, and resemble those made at the much more sophisticated level of theory, full π CASSCF/6-311G(2d,p) (the rms-difference between the optimized bond lengths in phenoxyl radical at the UMP2/6-31G** and π CASSCF(7,7)/6-311G(2d,p) levels is 0.010 Å).[51a] This unexpected result suggests that dynamic electron correlation (which is neglected at the CASSCF(2,2) level, almost neglected at the π CASSCF(7,7) level and partially taken into account at the UMP2 level) does not significantly affect the valence bond

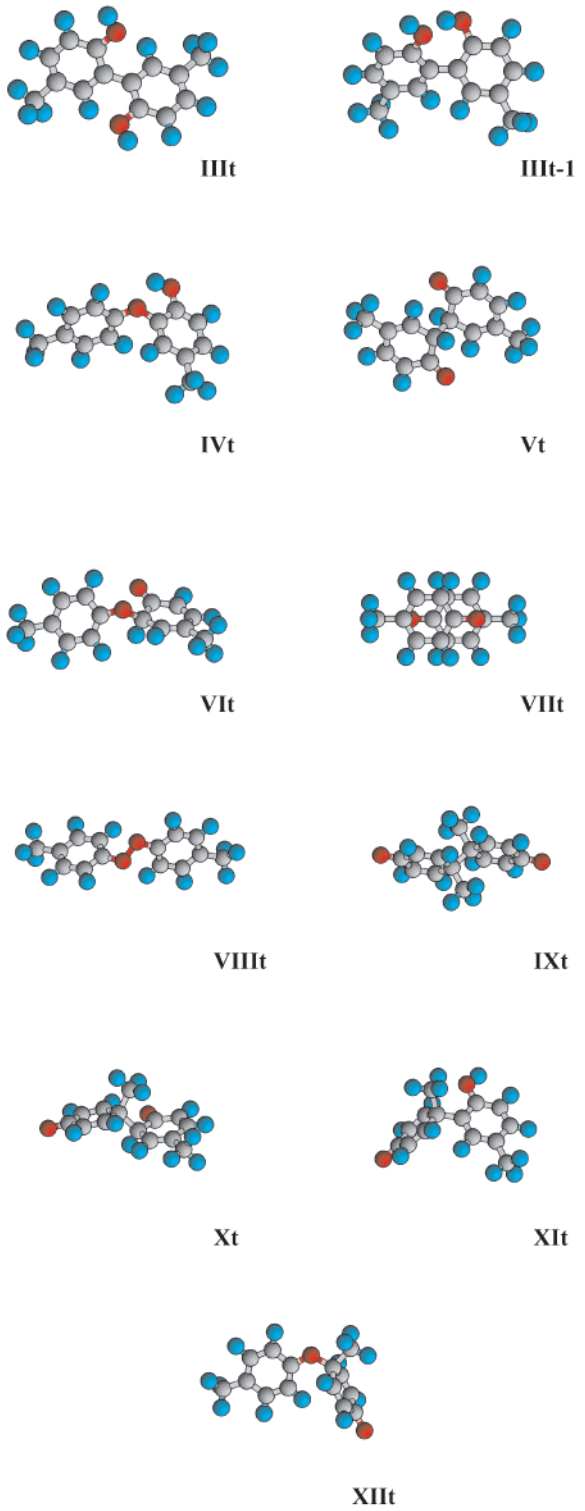

Figure 6. Optimal geometries of products and reaction intermediates of tyrosine coupling obtained by B3LYP/6-31G** calculations. Tyrosine was simulated by *p*-cresol. Structure of **VIIt** was obtained by full geometry optimization at the MP2/6-31G** level. Gray, red, and blue spheres designate carbon, oxygen, and hydrogen atoms, respectively.

lengths in the radical. On the other hand, static electron correlation, which is not properly taken into account within the UHF and UB3LYP approaches,[43,71] appears to be essential for geometry of phenoxyl system, as observed by the large difference in geometric predictions made at the UHF and UB3LYP levels versus those made at the CASSCF(2,2) level. The latter approach treats two noninteracting phenoxyl radicals as a singlet diradical, i.e., in such a way that the resulting HF

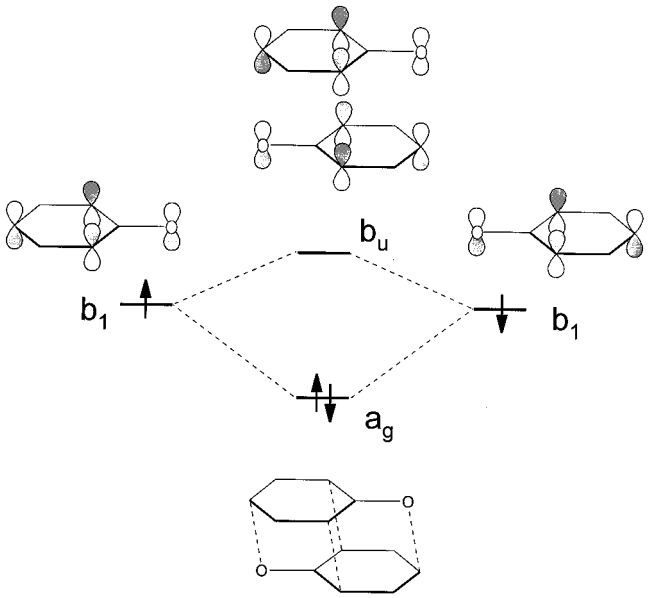

Figure 7. Orbital diagram demonstrating the origin of the HOMO and LUMO orbitals in stacked diphenoxyl (**VIIp**).

wave function of the system corresponds to a pure singlet state.[43] This result is consistent with recent studies of the excited singlet and triplet states of tyrosine, which demonstrated the importance of the static electron correlation effects for geometry of these species.[45]

As far as the stacked diphenoxyl structure is concerned, geometric predictions made by the different methods also split into two categories, but in a different way (Figure 10). Specifically, methods CASSCF(2,2) and HF predict similar geometric features of the dimer, which differ from those predicted by MP2 and B3LYP. This confirms that the only advantage of the CASSCF(2,2) approach over the HF is that it recovers static electron correlation effects in radical species. The similarity between the MP2 and B3LYP geometric predictions in the dimer is in agreement with the noticed analogous ability of these methods to recover dynamic electron correlation effects in closed-shell systems.[43,51g,51j] The characteristic split of the geometric predictions in **II** and **VII** made by different theoretical methods is consistent with the dominant role of the HOMO electron pair in dynamic electron correlation effects. This result basically coincides with the conclusion made above when reproducing the experimentally observed OH bond strength in phenol using different ab initio methods. Consistent with previous studies, dynamic electron correlation more significantly affects stability and geometric features of the close- than the open-shell systems.[43,61] These considerations also suggest that UMP2 is the only method utilized which is acceptable for geometric predictions of both phenoxyl radical and stacked diphenoxyl (Figure 10). Thus, the geometric changes in phenoxyl radical upon stacking dimerization are predicted to lead to a decrease of the "bond length alternation", i.e., toward the benzenoid ring character.

The observed similarity of the CASSCF(2,2) and HF methods in bond length predictions within phenoxyl moieties of the dimer **VII** extends to the other features of the dimer (Table 4). The inter-plane distance (δ) and mutual orientation of the phenoxyl units within the dimer measured by the distances (C(o)−C(o′)) and (O−C(p′)) are also very similar. As one would expect, dynamic electron correlation effects in **VII** recovered at the MP2/6-31G** level lead to a more compact arrangement of the

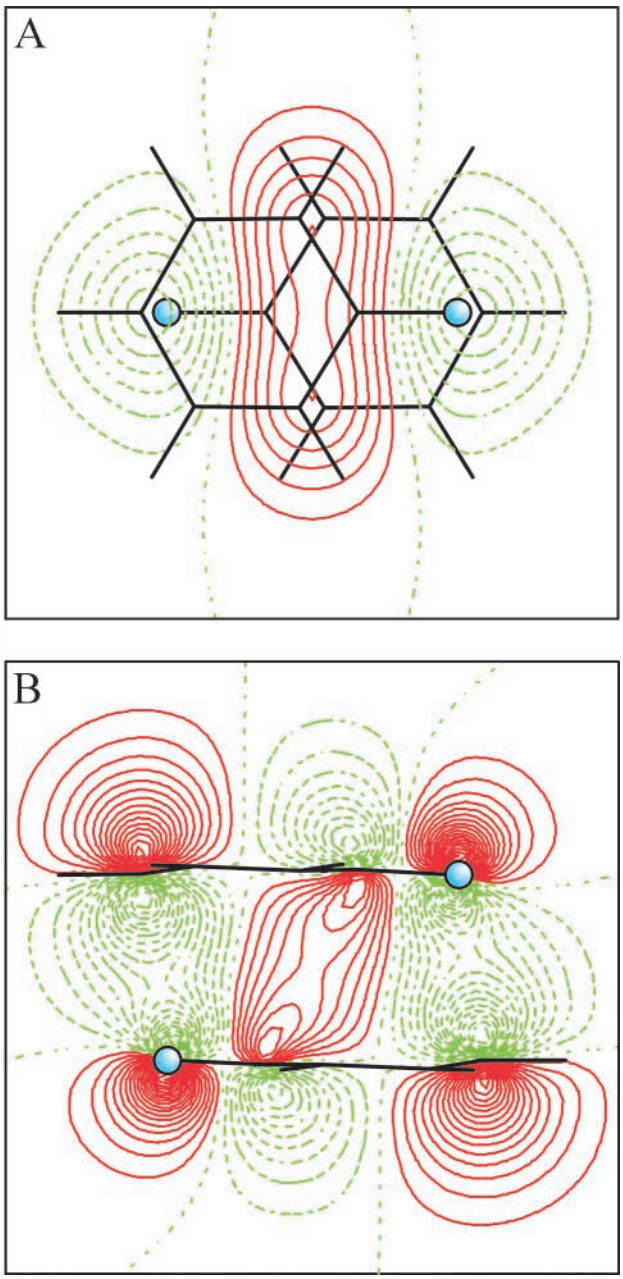

Figure 8. The HOMO of stacked diphenoxyl (**VIIp**) determined at the HF/6-31G** level using the MP2/6-31G** optimized geometry shown in two orthogonal planes. A − within the middle plane between the phenoxyl moieties; B − within the plane of symmetry. Solid black lines illustrate molecular geometry. Red lines signify positive values of MO; broken green lines signify negative values. Blue spheres designate oxygen atoms. It is seen that the HOMO is delocalized over 10 atoms, therefore the critical role of dynamic correlation effects of the HOMO electron pair is expected.

phenoxyl moieties. Particularly, this concerns the O−C(p′) distance in **VII**, which is predicted by the MP2 approach to be 0.273 Å shorter than predicted at the HF/6-31G** level. Theoretical approaches which are not able to take dynamic electron correlation within the valence shell of the stacked dimer into account, namely HF, CASSCF(2,2), CASSCF(10,10), and B3LYP, underestimate chemical bonding between two phenoxyl units in **VII** and suggest only the van der Waals type interaction. This is clearly seen in the predicted equilibrium interatomic separation C(o)−C(o′) in the dimer (2.7−2.8 Å) which is rather close to the sum of van der Waals radii of carbon atoms (2.9−3.0 Å[72]).

TABLE 4: Dimerization Energy and Selected Geometric Features of Stacked Diphenoxyl (VIIp) Predicted by ab Initio Calculations[a]

level of theory[b]	energy kJ/mol	interatomic distances[c], Å (C−O)	C−O	o−o′	O−p′	δ
ROHF/6-31G**	86.8	(1.329)	1.216	2.694	2.728	2.67
UHF/6-31G**	266.0	(1.254)	1.216	2.694	2.728	2.67
PUHF/6-31G**	518.1	(1.254)	1.216	2.694	2.728	2.67
UMP2/6-31G**	−330.2	(1.225)	1.264	2.543	2.455	2.52
PUMP2/6-31G**	−129.2	(1.225)	1.264	2.543	2.455	2.52
CASSCF(2,2)/6-31G**	−18.7	(1.208)	1.224	2.710	2.740	2.68
CASPT2(2,2)/6-31G**// CASSCF(2,2)/6-31G**	−65.8	(1.208)	1.224	2.710	2.740	2.68
CASSCF(10,10)/6-31G*	∼ −7.0	(1.256)	N/C	>2.8		
B3LYP/6-31G**	−15.9	(1.258)	1.248	2.765	2.693	2.74

[a] Energy of two isolated phenoxyl radicals (**IIp**) was considered as zero. [b] The active space within the CASSCF(2,2) approximation included two π-orbitals (HOMO and LUMO) of **VIIp** (Figure 7). The active space of the CASSCF(10,10) level was formed from five inner π-MO of each phenoxyl unit. [c] Bond length C−O, distances between ortho-carbon atoms (o−o′), between oxygen and para-carbon atoms (O−p′) and between the mean planes of the phenoxyl moieties (δ) within **VIIp** are presented. The value in parentheses gives the corresponding C−O bond length in phenoxyl radical. N/C − geometry optimization convergency was not achieved. The BSSE correction is not shown. Large variations in stabilization energy predicted by different methods suggest that further investigation of the stacked diphenoxyl system by other ab initio methods which more rigorously treat strong dynamic electron correlation effects is required.

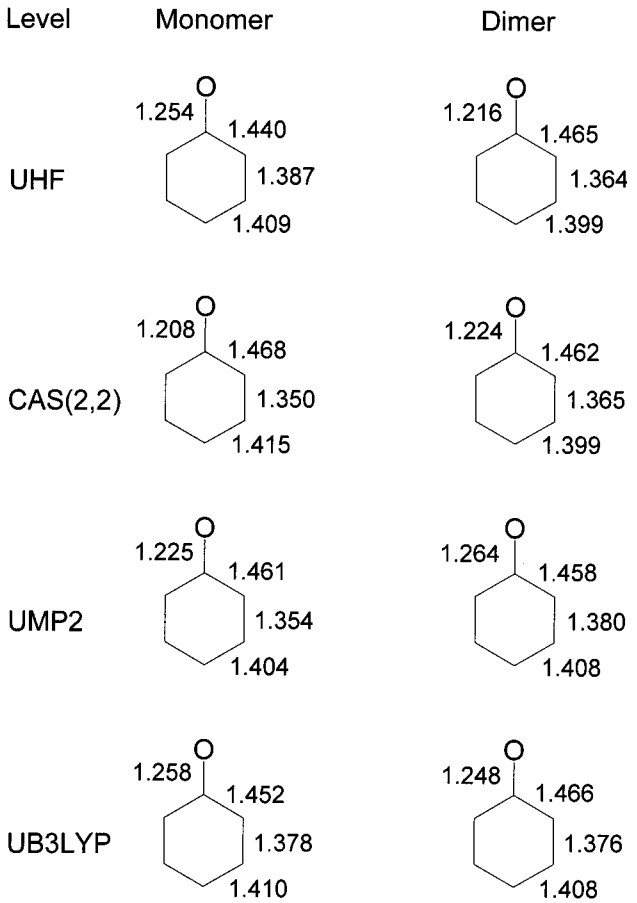

Figure 9. Optimized bond lengths (in Å) in phenolic units of phenoxyl radical (monomer, **IIp**) and stacked diphenoxyl (dimer, **VIIp**) obtained at the indicated levels of theory.

Inhibition of Tyrosine Coupling. It is established that coupling of tyrosyl radicals does not occur under acidic conditions.[24,28,39,65] Since no explanation for this observation

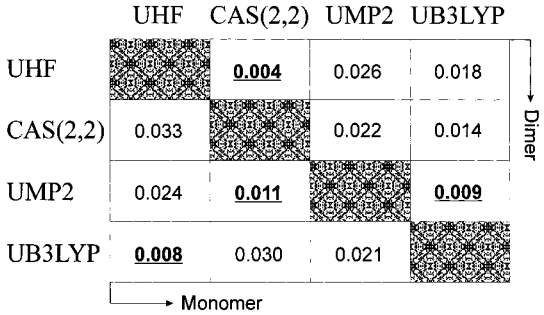

Figure 10. The rms-difference of bond lengths predicted by different ab initio methods for phenoxyl radical (monomer, **IIp**, lower triangle) and stacked diphenoxyl (dimer, **VIIp**, higher triangle). The bolded underlined values indicate geometric similarity.

has been reported to date, we investigated the reason for the pH dependence of tyrosine coupling based on theoretical considerations. According to cyclic voltammetry and EPR spectroscopic measurements under acidic conditions, tyrosyl radical interacts with proton and forms tyrosyl radical cation ([Tyr-OH$^{\bullet}$]$^{+}$).[63,73] Proton affinity of phenoxyl radical in the gas phase is estimated to be approximately 9.5 and 9.3 eV at the fully optimized UB3LYP/6-31G** and PUMP2/6-31G** levels of theory, respectively. These values are between the proton affinity of imidazole (the heterocyclic ring of His) which is estimated to be 10.4 and 10.3 eV at the same levels of theory, and that of H_2O, which is predicted to be 7.8 eV. Estimates of proton affinities have been found to depend on basis set and are exaggerated at the 6-31G** level.[74] Thus, experimentally determined proton affinity of H_2O in the gas phase is 7.16 ± 0.02 eV.[75] Nevertheless, the predicted trend remains valid since the utilized basis set has been found to result in systematic errors to proton affinities within a broad set of molecules.[74] These considerations suggest that a tyrosyl radical becomes protonated under more acidic conditions than His, i.e., at pH < 6. Under these conditions, the electrostatic repulsion between tyrosyl radical cations will decrease the probability of their direct contact and, thereby, inhibit their chemical coupling undergoing through reaction pathway 2, consistent with observations.[24,28]

Conclusions

The multireference CASSCF approach which involves only π-orbitals considerably underestimates dynamic electron correlation effects in closed-shell molecules related to phenol, which is manifested by modulation in geometry and energy of radical reactions, suggesting a critical role of $\sigma-\pi$ correlation. The ideal method for such systems would be CASPT2 which takes into account dynamic electron correlation and is free of spin contamination, but it is demonstrated that the "projected" single-reference PUMP2 method is sufficient enough for practical purposes. Consistent with previous observations, the DFT approach underestimates the stabilization energy of the stacking complexes of planar molecules.

The fully relaxed ab initio calculations at the B3LYP and MP2 levels demonstrate that the observed products of tyrosine coupling (dityrosine and isodityrosine) are the most stable dimers of tyrosine. In addition to classical reaction intermediates which have been postulated for phenol coupling processes, a novel transient structure, stacked dityrosyl, is predicted. Stacked dityrosyl is unstable at the HF level, and, therefore, stabilized exclusively by electron correlation.

Acknowledgment. This work was supported by a research grant from Neuroceptor Inc. (Ontario, Canada) and by operating grants to R.J.R. and G.M.R. from the Canadian Institutes of Health Research. G.M.R. is a Queen's National Scholar.

References and Notes

(1) Raina, A. K.; Perry, G.; Nunomura, A.; Sayre, L. M.; Smith, M. A. *Clin. Chem. Lab. Med.* **2000**, *38*, 93−97.
(2) Squier, T. C.; Bigelow, D. J. *Front. Biosci.* **2000**, *5*, D504−D526.
(3) Cracowski, J. L.; Stanke-Labesque, F.; Souvignet, C.; Bessard, G. *Presse Med.* **2000**, *29*, 604−610.
(4) Allen, R. G.; Tresini, M. *Free Radical Biol. Med.* **2000**, *28*, 463−499.
(5) Christen, Y. *Am. J. Clin. Nutr.* **2000**, *71*, 621S−629S.
(6) Mattson, M. P.; Pedersen, W. A.; Duan, W.; Culmsee, C.; Camandola, S. *Ann. N.Y. Acad. Sci.* **1999**, *893*, 154−175.
(7) Spitz, D. R.; Sim, J. E.; Ridnour, L. A.; Galoforo, S. S.; Lee, Y. J. *Ann. N.Y. Acad. Sci.* **2000**, *899*, 349−362.
(8) Yokoyama, M.; Inoue, N.; Kawashima, S. *Ann. N.Y. Acad. Sci.* **2000**, *902*, 241−248.
(9) Floyd, R. A. *Proc. Soc. Exp. Biol. Med.* **1999**, *222*, 236−245.
(10) (a) Juurlink, B. H. *Neurosci. Biobehav. Rev.* **1997**, *21*, 151−166. (b) Juurlink, B. H.; Sweeney, M. I. *Neurosci. Biobehav. Rev.* **1997**, *21*, 121−128.
(11) Robberecht, W. *J. Neurol.* **2000**, *247*, Suppl. 1, I1−I6.
(12) Smith, K. J.; Kapoor, R.; Felts, P. A. *Brain Pathol.* **1999**, *9*, 69−92.
(13) Offen, D.; Hochman, A.; Gorodin, S.; Ziv, I.; Shirvan, A.; Barzilai, A.; Melamed, E. *Adv. Neurol.* **1999**, *80*, 265−269.
(14) Grunewald, T.; Beal, M. F. *Ann. N.Y. Acad. Sci.* **1999**, *893*, 203−213.
(15) Pennathur, S.; Jackson-Lewis, V.; Przedborski, S.; Heinecke, J. W. *J. Biol. Chem.* **1999**, *274*, 34621−34628.
(16) Evans, P. H. *Br. Med. Bull.* **1993**, *49*, 577−587.
(17) La Voie, M. J.; Hastings, T. G. *J. Neurochem.* **1999**, *73*, 2546−2554.
(18) Spencer, J. P. E.; Jenner, P.; Daniel, S. E.; Lees, A. J.; Marsden, D. C.; Halliwell, B. *J. Neurochem.* **1998**, *71*, 2112−2122.
(19) Merenyi, G.; Lind, J.; Czapski, G.; Goldstein, S. *Proc. Natl. Acad. Sci. U.S.A.* **2000**, *97*, 8216−8218.
(20) Cudic, M.; Ducrocq, C. *Nitric Oxide* **2000**, *4*, 147−156.
(21) Zhang, H.; Joseph, J.; Felix, C.; Kalyanaraman, B. *J. Biol. Chem.* **2000**, *275*, 14038−14045.
(22) Santos, C. X.; Bonini, M. G.; Augusto, O. *Arch. Biochem. Biophys.* **2000**, *377*, 146−152.
(23) Tsai, H.-H.; Hamilton, T. P.; Tsai, J.-H.; van der Woerd, M.; Harrison, J. G.; Jablonsky, M. J.; Beckman, J. S.; Koppenol, W. H. *J. Phys. Chem.* **1996**, *100*, 15087−15095.
(24) Jacob, J. S.; Cistola, D. P.; Hsu, F. F.; Muzaffar, S.; Mueller, D. M.; Hazen, S. L.; Heinecke, J. W. *J. Biol. Chem.* **1996**, *271*, 19950−19956.
(25) Alexi, T.; Borlongan, C. V.; Faull, R. L.; Williams, C. E.; Clark, R. G.; Gluckman, P. D.; Hughes, P. E. *Prog. Neurobiol.* **2000**, *60*, 409−470.
(26) Diner, B. A.; Force, D. A.; Randall, D. W.; Britt, R. D. *Biochemistry* **1998**, *37*, 17931−17943.
(27) Xiao, G.; Tsai, A. L.; Palmer, G.; Boyar, W. C.; Marshall, P. J.; Kulmacz, R. J. *Biochemistry* **1997**, *36*, 1836−1845.
(28) Spikes, J. D.; Shen, H. R.; Kopeckova, P.; Kopecek, J. *Photochem. Photobiol.* **1999**, *70*, 130−137.
(29) Babcock, G. T.; Espe, M.; Hoganson, C.; Lydakis-Simantiris, N.; McCracken, J.; Shi, W.; Styring, S.; Tommos, C.; Warncke, K. *Acta Chem. Scand.* **1997**, *51*, 533−540.
(30) Galeazzi, L.; Ronchi, P.; Franceschi, C.; Giunta, S. *Amyloid* **1999**, *6*, 7−13.
(31) Pfeiffer, S.; Schmidt, K.; Mayer, B. *J. Biol. Chem.* **2000**, *275*, 6346−6352.
(32) Lardinois, O. M.; Medzihradszky, K. F.; de Montellano, O. P. R. *J. Biol. Chem.* **1999**, *274*, 35441−35448.
(33) Leeuwenburgh, C.; Hansen, P. A.; Holloszy, J. O.; Heinecke, J. W. *Am. J. Physiol.* **1999**, *276*, R128−R135.
(34) Goldstein, S.; Czapski, G.; Lind, J.; Merenyi, G. *J. Biol. Chem.* **2000**, *275*, 3031−3036.
(35) Baudry, N.; Lejeuna, P. J.; Niccoli, P.; Vinet, L.; Carayon, P.; Mallet, B. *FEBS Lett.* **1996**, *396*, 223−226.
(36) Souza, J. M.; Giasson, B. I.; Chen, Q.; Lee, V. M.; Ischiropoulos, H. *J. Biol. Chem.* **2000**, *275*, 18344−18349.
(37) Brady, J. D.; Sadler, I. H.; Fry, S. C. *Phytochemistry* **1998**, *47*, 349−353.
(38) Leeuwenburgh, C.; Hansen, P. A.; Holloszy, J. O.; Heinecke, J. W. *Free Radical Biol. Med.* **1999**, *27*, 186−192.
(39) Brunow, G.; Kilpeläinen, I.; Sipilä, J.; Syrjänen, K.; Karhunen, P.; Setälä, H.; Rummakko, P. In *Lignin and Lignan Biosynthesis*; Lewis, N. G., Sarkanen, S., Eds.; ACS Symp. Ser. Vol. 697, Am. Chem. Soc.: Washington, DC, 1998; pp 131−147.

(40) Nakagawa, H.; Sumiki, E.; Takusagawa, M.; Ikota, N.; Matsushima, Y.; Ozawa, T. *Chem. Pharm. Bull. (Tokyo)* **2000**, *48*, 261−265.
(41) Guyton, K. Z.; Kensler, T. W. *Br. Med. Bull.* **1993**, *49*, 523−544.
(42) (a) Von Szentpály, L.; Shamovsky, I. L. *Mol. Pharmacol.* **1995**, *47*, 624−629. (b) Von Szentpály, L.; Shamovsky, I. L. *Int. J. Quantum Chem.: Quantum Biol. Symp.* **1995**, *22*, 191−199. (c) Von Szentpály, L.; Ghosh, R. In *Theoretical Organic Chemistry*; Párkányi, C., Ed.; Elsevier: New York, 1998; Vol. 5, pp 447−499.
(43) Bally, T.; Borden, W. T. In *Reviews in Computational Chemistry*; Lipkowitz, K. B., Boyd, D. B., Eds.; John Wiley and Sons: New York, 1999; Vol. 13, pp 1−97.
(44) (a) Liu, R.; Zhou, X. *Chem. Phys. Lett.* **1993**, *207*, 185−189. (b) Liu, R.; Zhou, X. *J. Phys. Chem.* **1993**, *97*, 9613−9617. (c) Chipman, D. M.; Liu, R.; Zhou, X.; Pulay, P. *J. Chem. Phys.* **1994**, *100*, 5023−5035.
(45) (a) Hameka, H. F.; Jensen, J. O. *J. Mol. Struct.* **1993**, *288*, 9−16. (b) Samuels, A. C.; Jensen, J. O.; Hameka, H. F. *J. Mol. Struct. (THEOCHEM)* **1998**, *454*, 25−30.
(46) Parr, R. F.; Yang, W. *Density Functional Theory of Atoms and Molecules*; Oxford University: New York, 1989.
(47) *Density Functional Methods in Chemistry*; Labanowski, J. K., Andzelm, J. W., Eds.; Springer-Verlag: New York, 1991.
(48) Frisch, M. J.; Pople, J. A.; Binkley, J. S. *J. Chem. Phys.* **1984**, *80*, 3265.
(49) Lee, C.; Yang, W.; Parr, R. G. *Phys. Rev. B* **1988**, *37*, 785−789.
(50) Becke, A. D. *J. Chem. Phys.* **1993**, *98*, 5648−5652.
(51) (a) Qin, Y.; Wheeler, R. A. *J. Chem. Phys.* **1995**, *102*, 1689−1698. (b) Li, J.; Fisher, C. L.; Chen, J. L.; Bashford, D.; Noodleman, L. *Inorg. Chem.* **1996**, *35*, 4694−4702. (c) Pudzianowski, A. T. *J. Phys. Chem.* **1996**, *100*, 4781−4789. (d) Jalkanen, K. J.; Suhai, S. *Chem. Phys.* **1996**, *208*, 81−116. (e) Nwobi, O.; Higgins, J.; Zhou, X.; Liu, R. *Chem. Phys. Lett.* **1997**, *272*, 155−161. (f) Kumar, G. A.; McAllister, *J. Am. Chem. Soc.* **1998**, *120*, 3159−3165. (g) Paizs, B.; Suhai, S. *J. Comput. Chem.* **1998**, *19*, 575−584. (h) Han, W.-G.; Jalkanen, K. J.; Elstner, M.; Suhai, S. *J. Phys. Chem. B* **1998**, *102*, 2587−2602. (i) Kieninger, M.; Suhai, S.; Ventura, O. N. *J. Mol. Struct. (THEOCHEM)* **1998**, *433*, 193−201. (j) Hobza, P.; Šponer, J. *Chem. Rev.* **1999**, *99*, 3247−3276. (k) Cohen, A. J.; Handy, N. C. *Chem. Phys. Lett.* **2000**, *316*, 160−166.
(52) Møller, C.; Plesset, M. S. *Phys. Rev.* **1934**, *46*, 618.
(53) Head-Gordon, M.; Pople, J. A.; Frisch, M. J. *Chem. Phys. Lett.* **1988**, *153*, 503−506.
(54) (a) Hegarty, D.; Robb, M. A. *Mol. Phys.* **1979**, *38*, 1795. (b) Eade, R. H. E.; Robb, M. A. *Chem. Phys. Lett.* **1981**, *83*, 362.
(55) Andersson, K.; Roos, B. O. In *Modern Electronic Structure Theory, Part 1*, Advanced Series in Physical Chemistry, Vol. 2; Yarkony, D. R., Ed.; Singapore: World Scientific, 1995; pp 55−109.
(56) Roothaan, C. C. J. *Rev. Mod. Phys.* **1960**, *32*, 179.
(57) Pople, J. A.; Nesbet, R. K. *J. Chem. Phys.* **1954**, *22*, 571.
(58) Löwdin, P.-O. *Phys. Rev.* **1955**, *97*, 74.
(59) (a) Jansen, H. B.; Ross, P. *Chem. Phys. Lett.* **1969**, *3*, 140. (b) Boys, S. B.; Bernardi, F. *Mol. Phys.* **1970**, *19*, 553. (c) Van Duijneveldt, F. B., et al. *Chem. Rev.* **1994**, *94*, 1873−1885.
(60) Frisch, M. J.; Trucks, G. W.; Schlegel, H. B.; Scuseria, G. E.; Robb, M. A.; Cheeseman, J. R.; Zakrzewski, V. G.; Montgomery, J. A., Jr.; Stratmann, R. E.; Burant, J. C.; Dapprich, S.; Millam, J. M.; Daniels, A. D.; Kudin, K. N.; Strain, M. C.; Farkas, O.; Tomasi, J.; Barone, V.; Cossi, M.; Cammi, R.; Mennucci, B.; Pomelli, C.; Adamo, C.; Clifford, S.; Ochterski, J.; Petersson, G. A.; Ayala, P. Y.; Cui, Q.; Morokuma, K.; Malick, D. K.; Rabuck, A. D.; Raghavachari, K.; Foresman, J. B.; Cioslowski, J.; Ortiz, J. V.; Baboul, A. G.; Stefanov, B. B.; Liu, G.; Liashenko, A.; Piskorz, P.; Komaromi, I.; Gomperts, R.; Martin, R. L.; Fox, D. J.; Keith, T.; Al-Laham, M. A.; Peng, C. Y.; Nanayakkara, A.; Gonzalez, C.; Challacombe, M.; Gill, P. M. W.; Johnson, B.; Chen, W.; Wong, M. W.; Andres, J. L.; Gonzalez, C.; Head-Gordon, M.; Replogle, E. S.; Pople, J. A. *Gaussian-98, Revision A.7;* Gaussian, Inc.: Pittsburgh, PA, 1998.
(61) Hehre, W. J.; Radom, L.; Schleyer, P.v. R.; Pople, J. A. *Ab Initio Molecular Orbital Theory*; New York: Wiley-Interscience: 1986.
(62) *Handbook of Chemistry and Physics*, 81st ed.; Lide, D. R., Ed.; CRC Press: Boca Raton, FL, 2000−2001.
(63) Harriman, A. *J. Phys. Chem.* **1987**, *91*, 6102−6104.
(64) Zhang, H.; Squadrito, G. L.; Uppu, R.; Pryor, W. A. *Chem. Res. Toxicol.* **1999**, *12*, 526−534.
(65) van der Vliet, A.; Eiserich, J. P.; O'Neill, C. A.; Halliwell, B.; Cross, C. E. *Arch. Biochem. Biophys.* **1995**, *319*, 341−349.
(66) Epperlein, M. M.; Nourooz-Zadeh, J.; Jayasena, S. D.; Hothersall, J. S.; Noronha-Dutra, A.; Neild, G. H. *J. Am. Soc. Nephrol.* **1998**, *9*, 457−463.
(67) Bonini, M. G.; Radi, R.; Ferrer-Sueta, G.; Ferreira, A. M.; Augusto, O. *J. Biol. Chem.* **1999**, *274*, 10802−10806.
(68) Polanyi, J. C. *Science* **1987**, *236*, 680.
(69) (a) Kristyán, S.; Pulay, P. *Chem. Phys. Lett.* **1994**, *229*, 175. (b) Pérez-Jordá, J. M.; Becke, A. D. *Chem. Phys. Lett.* **1995**, *233*, 134. Hobza, P.; Šponer, J.; Reschel, T. *J. Comput. Chem.* **1995**, *16*, 1315. (d) Dudzianowski, A. T. *J. Phys. Chem.* **1996**, *100*, 4781.
(70) Šponer, J.; Leszczynski, J.; Hobza, P. *J. Comput. Chem.* **1996**, *17*, 841.
(71) (a) Bofill, J. M.; Pulay, P. *J. Chem. Phys.* **1989**, *90*, 3642. (b) Yu, H.; Goddard, J. D. *J. Mol. Struct. (THEOCHEM)* **1991**, *233*, 129.
(72) Ramachandran, G. N.; Sasisekharan, V. *Adv. Protein Chem.* **1968**, *23*, 326.
(73) Mino, H.; Kawamori, A.; Ono, T. *Biochim. Biophys. Acta* **2000**, *1457*, 157−165.
(74) Smith, B. J. In *Encyclopedia of Computational Chemistry*, Vol. 3; Schleyer, P.v. R., Ed.; John Wiley and Sons: Chichester-New York, 1998; pp 2270−2283.
(75) Szulejko, J. E.; McMahon, T. B. *J. Am. Chem. Soc.* **1993**, *115*, 7839−7848.